Journal of Applied Electrochemistry **32**: 287–295, 2002.

High specific surface area, reticulated current collectors for lead–acid batteries

E. GYENGE[1]*, J. JUNG[1], S. SPLINTER[1] and A. SNAPER[2]
[1]*BC Research Inc. and Power Technology Research and Development Laboratory, 3650 Wesbrook Mall, Vancouver, BC, Canada V6S 2L2*
[2]*Power Technology Inc., 1000 West Bonanza Road, Las Vegas, Nevada, USA*
*(*author for correspondence, fax: 1 604 224 0540, e-mail: egyenge@bcresearch.com)*

Received 6 August 2001; accepted in revised form 12 February 2002

Key words: lead–acid battery, reticulated grid, utilization efficiency

Abstract

The use of high specific surface area (>10 cm^2 cm^{-3}) reticulated current collectors in lead–acid batteries was studied by cyclic voltammetry, 2 V battery testing and scanning electron microscopy (SEM). Comparative cyclic voltammetry experiments revealed differences in the electrochemical behaviour of reticulated and book-mould current collector designs, with regard to both $PbSO_4$ and PbO_2 film formation. Battery testing showed that the electrochemical utilization efficiency of the positive active material (PAM) in flooded cells equipped with about 10 pores cm^{-1} reticulated collectors was between 30 and 50% higher than for the book-mould grid battery at discharge rates from 5 to 3 h. For instance, at the 3 h rate the PAM utilization efficiency was 45% and the capacity was 101 Ah (kg PAM)$^{-1}$ for reticulated collectors as opposed to 29.5% and 66 Ah (kg PAM)$^{-1}$, respectively, for a battery equipped with conventional grids. The results were attributed to differences in PAM morphology as shown by SEM micrographs.

1. Introduction

The lead–acid battery in its various configurations is a time-honored power source for diverse applications such as starting–lighting–ignition (SLI), uninterrupted power supply (UPS) and motive power. Continuous developments on the application side, for instance in the area of electric and hybrid vehicles (EV and HEV), impose challenging performance demands on battery technologies in general and lead–acid batteries in particular [1–3]. The performance targets for EV use set by the Advanced Lead Acid Battery Consortium (ALABC) are summarized as follows: specific energy 50 Wh kg^{-1} at $C/3$ discharge rate, specific power 150 W kg^{-1} at 80% depth-of-discharge (DoD) and fast recharging (e.g., 80% charge in 15 min) [4]. To meet these objectives, a 'systems approach' to battery research and development involving all components, such as current collector structure, paste composition, charging protocol and charger design, thermal and electrolyte management and overall battery configuration (e.g., monopolar or bipolar) is required.

Improvements to the current collector have been made with regard to both alloy composition and grid design (e.g., expanded mesh) [1, 5]. Fast charging techniques however, require the use of high current densities per geometric current collector area (e.g., $\geqslant$30 mA cm^{-2} [6]), which can facilitate the occurrence of side reactions such as prohibitively high H_2 and O_2 evolution rates and accelerated corrosion of the positive current collector.

During discharge, on the other hand, it is well-known that the low utilization efficiency of the active mass, especially on the positive electrode limits the actual specific energy of the lead–acid battery. Typical positive active material (PAM) utilization efficiencies range between 25 and 40% for traction batteries at 5 h rate [1]. It is generally accepted that the microstructure of the current collector plays an important role in determining the electrochemical utilization efficiency of PAM. The current collector structure must allow for significant (e.g., ~50%) volume increase during discharge, while maintaining adequate electrical contact with the active material particles and assuring efficient ion transport to the electroactive sites [7].

About thirty years ago, Faber showed that reducing the dimensions of grid openings brings about an increase of active material utilization. For grid mesh openings below 1 mm, utilization efficiencies above 60% were obtained, while fiber type of grid structures with openings of about 0.1 mm, yielded above 90% active mass utilization [8]. In spite of these findings, there have been relatively few subsequent reports on the relationship between grid design and utilization efficiency. The research effort focused mainly on different paste formulations, which could lead to improved PAM utilization [9].

In a comprehensive study of the grid/PAM interface, Pavlov introduced the γ parameter, which reflects the

importance of the effective grid surface area, S_{grid}, in relation to the PAM weight, W_{PAM} [10]:

$$\gamma = \frac{W_{PAM}}{S_{grid}} \quad (1)$$

The γ parameter depends on the design of the plate and has an important effect on the rates of interfacial processes. For improvements in both PAM utilization efficiency and cycle life of SLI batteries, plates with γ factors of 0.5 – 0.8 g_{PAM} cm^{-2} were proposed [10].

A reticulated, open-cell electrode structure characterized by high specific surface area and porosity (typically 10 – 100 cm^2 cm^{-3} and 90 – 97%, respectively), provides a large effective contact area for the active material (e.g., $\gamma \leqslant 0.5$ g_{PAM} cm^{-2}), which in turn could improve the active material utilization efficiency and the specific energy of lead–acid battery.

There are only a few reports on the use of reticulated current collectors in lead–acid batteries. Czerwinski and Zelazowska investigated the fundamental electrochemical behaviour of Pb and PbO_2 deposited on reticulated vitreous carbon [11, 12]. Based on cyclic voltammetry studies, it was concluded that the reticulated carbon substrate had no negative influence on the performance of the active materials. However, the potential benefits of a high specific surface area current collector were not established. Furthermore, no experimental data were presented detailing the behaviour of the deposited reticulated electrodes in lead–acid batteries.

The use of reticulated current collector structures for battery applications was claimed by Snaper in US Patent 6 060 198 and assigned to Power Technology Inc. [13]. Recently, Arias et al. evaluated reticulated lead current collectors in conjunction with a sulfate-based paste and a novel three-step charging method. It was found that the reticulated lead structure yielded positive active mass utilization efficiencies of 56% at 4 mA cm^{-2} and 30% at 56 mA cm^{-2}, whilst under similar conditions a typical book-mould collector yielded 49% and 25% utilization efficiencies, respectively [14].

The goal of the present study was to investigate the behaviour of the reticulated lead structures by employing both cyclic voltammetry and battery testing experiments. Comparative studies were performed using standard book-mould collectors subjected to the same experimental protocols.

2. Experimental methods

The reticulated current collectors were manufactured by casting, using a Pb–Ca–Al alloy of similar composition as the conventional book-mould grid used in comparative experiments. Figure 1 shows scanning electron microscopy images (SEM) of the employed reticulated lead structures with approximately 10 pores cm^{-1}.

Cyclic voltammetry studies were conducted using an AMEL 2055 high-power potentiostat connected to a Pentium III PC via a PowerLab/4SP data acquisition board and Echem® 1.51 software (AD Instruments). The electrolyte was 600 ml of naturally aerated H_2SO_4 with a relative density of 1.28. The effective geometric area and dimensions of the 'working' electrodes for voltammetry were as follows: bare reticulated lead 3.3 cm^2 (i.e., 2.2 cm × 1.5 cm × 0.4 cm), and bare book-mould grid 11.9 cm^2 (i.e., 3 cm × 3.9 cm × 0.07 cm). The counter electrode was a graphite rod (effective area 10 cm^2). A mercurous sulfate electrode (MSE; Hg/Hg_2SO_4/H_2SO_4, relative density 1.3; +0.630 V vs NHE) connected through a Luggin capillary served as reference. According to the general convention in lead–acid battery research, the oxidation currents on the voltametric sweep are given with a positive sign, while the reduction currents are marked with a negative sign.

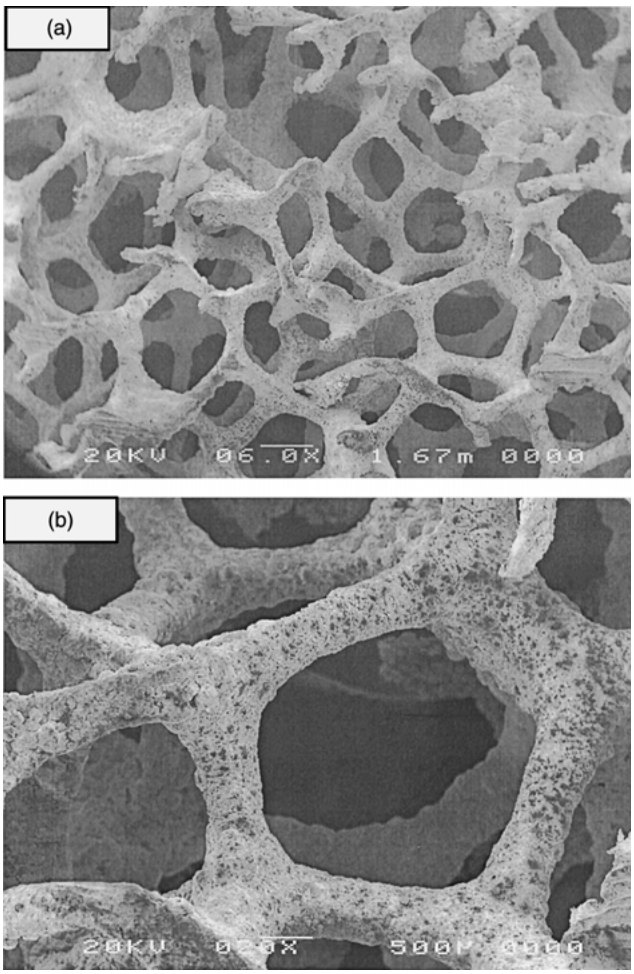

Fig. 1. Scanning electron microscopy images of the reticulated current collector.

For comparative testing, single-cell flooded lead–acid batteries were assembled with reticulated and book-mould grids, respectively. The grids were manually pasted using industry standard lead(II) oxide based paste, followed by curing at 45 °C. The physical characteristics of the employed single-cell batteries are given in Table 1.

Table 1. Physical characteristics of the battery plates

Current collector	Superficial area /cm^2	Specific surface area /cm^2 cm^{-3}	Collector weight per unit volume /g cm^{-3}	'Positive' dry paste mass /g	'Negative' dry paste mass /g
Reticulated (~10 pores cm^{-1})	68 (8.6 cm × 7.9 cm × 0.3 cm)	14*	2.4	75.3	74.8
Book-mould	162 (14.6 cm × 11.1 cm × 0.07 cm)	4.6†	5	53.3	61

* Estimate based on the reported specific surface area of reticulated vitreous carbon with the same number of pores [15].
† Estimate using the open-area factor for rectangular screens [16].

Table 1 shows that the apparent density of the collector was more than two times lower for reticulated lead. The specific surface area, on the other hand, was about three times higher, 14 cm^2 cm^{-3} compared with 4.6 cm^2 cm^{-3}, thus offering a more effective contact between active material and current collector. The amount of positive active material (PAM) per total estimated surface area, γ factor (Equation 1), was 0.3 g cm^{-2} for reticulated and 1.1 g cm^{-2} for book-mould collector, respectively.

The negative active mass was oversized for both batteries (Table 1) to determine the performance limiting effect of the positive active material. The cured plates were separated by pocket-type high-density microporous polyethylene and were placed in a plastic container. Forming was performed in H_2SO_4 15%w at current densities between 0.5 and 2 mA cm^{-2}, until a 20% excess against the theoretical charge of 241 Ah (kg PAM)$^{-1}$ was achieved. Using a low forming current density (e.g., 0.5 mA cm^{-2}) allows the reduction of the forming charge excess from about 50 – 60% to 20% or less [17]. A visual inspection of the plates showed complete forming under the employed conditions.

For cycling (charge–discharge) experiments, the electrolyte was H_2SO_4 with an initial relative density of 1.26. The acid volume was 140 ml. A three-step, constant current – constant voltage – equalization charge protocol was used, while the applied discharge currents ensured discharge rates of 5, 4 and 3 h, respectively. The batteries were operated at 295 K. The cut-off voltage was 1.4 V. At each discharge current density five replicated runs were performed.

The battery testing was performed using UBA4 battery analysers and software (Vencon Technologies) controlled by a Pentium III PC. The maximum current output per channel was 2 A for charge and 2.5 A for discharge, respectively.

3. Results and discussion

3.1. *Cyclic voltammetry of the reticulated and grid current collector structures*

Most of the literature information on the electrochemical behaviour of Pb and Pb alloys in H_2SO_4 was obtained from studies using flat plate or disc working electrodes. However, the design of the current collector (e.g., book-mould or reticulated structure) can have an important influence on various steps of the overall electrochemical process, such as crystallization, film formation and growth.

The cyclic voltammograms at 20 mV s^{-1} of the bare reticulated and book-mould structures are shown in Figure 2(a) and (b), respectively.

The Pb oxidation peak, a_1 – corresponding to $PbSO_4$ formation – occurs at virtually the same potential for the reticulated and conventional grid structures, (i.e., −0.86 and −0.88 V vs MSE, respectively). The corresponding superficial current density was about 20 times higher for the reticulated electrode. Based on the studies by Pavlov

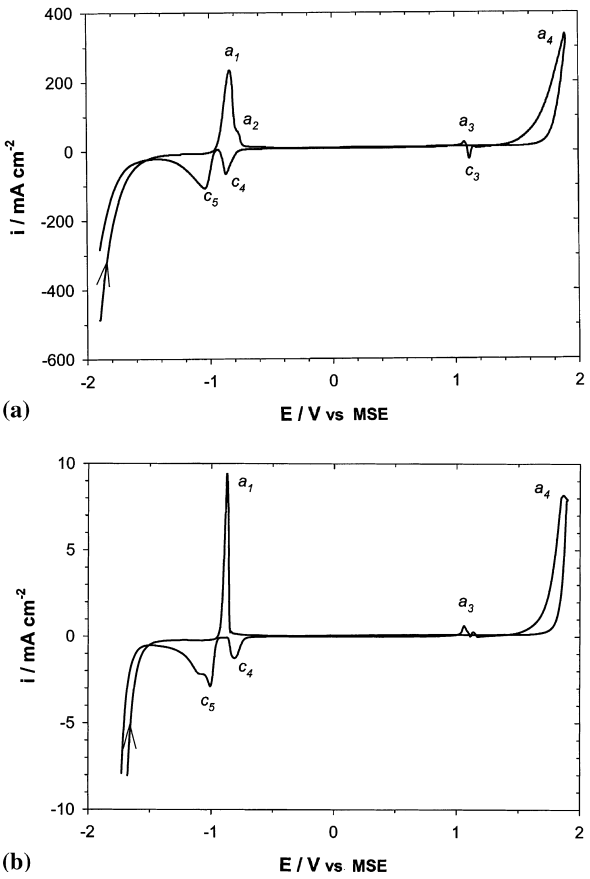

Fig. 2. Comparative cyclic voltammetry of the current collector structures. (a) Reticulated and (b) book-mould. Scan rate 20 mV s^{-1}; $T = 295$ K.

et al. and Ruetschi, it is accepted in the literature that in parallel with sulfate formation a PbO sublayer is generated beneath the $PbSO_4$ film as a result of impeded SO_4^{2-} and HSO_4^- diffusion to the reaction sites. The Pb^{2+} ions formed underneath the $PbSO_4$ layer are compensated by OH^- ions from H_2O dissociation, yielding PbO (i.e., selective permeation of the SO_4^{2-} 'membrane'). This phenomenon is sometimes referred to as stable passivation of lead (for a review see [18, 19] and original references therein).

However, in the case of the reticulated electrode at −0.79 V vs MSE, a shoulder-like anodic wave, a_2, was obtained, which was not observed for the book-mould structure (Figure 2(a)). Two consecutive anodic peaks at −0.8 and −0.6 V were reported for Pb in 0.1 M $Na_2B_4O_7$ ([11, 12] and references therein). The more negative peak was attributed to the formation of Pb^{2+} ions leading to lead borate while PbO generation was responsible for the peak occurring at the more positive potential. Therefore, it is proposed that on the reticulated electrode the oxidation of Pb to $PbSO_4$ and the generation of a PbO sublayer occur as two consecutive reactions instead of parallel processes.

Further on the anodic scan, small peaks – characteristic for the oxidation of $PbSO_4$ to PbO_2 – were found for both electrodes (peaks a_3 Figure 2(a) and (b)). In the case of the book-mould electrode, two consecutive peaks were obtained at 1.09 and 1.25 V, respectively (Figure 2(b)). The peak on the reticulated electrode occurred at 1.05 V (peak a_3 Figure 2(a)). It is known that at about 0.95 V α-PbO_2 is formed, while β-PbO_2 is generated at potentials above 1.0 V, the latter being more stable in acid. Generally, the mechanism of $PbSO_4$ oxidation is complex involving various intermediate species such as PbO, yPbO·PbSO$_4$ ($y = 1, \ldots, 4$), 5PbO·2H$_2$O and $PbOH^+$ [18, 20].

At potentials above 1.5 V both β-PbO_2 formation and O_2 evolution occur in parallel (e.g., wave a_4 Figure 2(a) and (b)). The corresponding current densities were as high as 300 mA cm^{-2} on the reticulated electrode compared to only 8 mA cm^{-2} on the conventional grid.

Differences between the two electrodes under study were also observed on the cathodic scan. A reduction peak at 1.1 V was detected on the reticulated electrode (peak c_3, Figure 2(a)), which was not observed for the book-mould collector (Figure 2(b)). The peak at 1.1 V belongs to the β-PbO_2/$PbSO_4$ couple [11]. Taking into account that the formation of β-PbO_2 is a slow reaction, the absence of the latter peak at 20 mV s^{-1} scan rate in the case of the conventional grid, indicates that during the time frame of one scan the amount of β-PbO_2 accumulated was small in comparison to the amount generated on the high-surface area, reticulated electrode.

Cathodic peaks were also obtained at potentials of −0.8 and −0.88 V for the book-mould and reticulated electrodes, respectively, (peak c_4, Figure 2(a) and (b)). These peaks were only observed when the electrode potential was cycled up to 1.9 V, that is, for anodized electrodes. The cathodic peaks at −0.8 and −0.88 V, are therefore representative for the reduction of the anodic films formed at positive potentials, namely PbO from yPbO·PbSO$_4$ ($y = 1, \ldots, 4$) [21].

At more negative potentials, around −1 V for both electrodes, $PbSO_4$ is reduced to metallic Pb (peaks c_5 Figure 2(a) and (b)).

3.2. *Cyclic voltammograms representative for the negative battery electrode*

The negative electrode of a flooded lead–acid battery is based on the $PbSO_4$/Pb redox couple (Equation 2). In the later stages of charging and during overcharge the reduction of $PbSO_4$ is less efficient and H_2 evolution occurs (Equation 3).

$$PbSO_4 + H^+ + 2e^- \rightleftharpoons Pb + HSO_4^- \quad (2)$$

$$2H^+ + 2e^- \rightarrow H_2(g) \quad (3)$$

The scan rate dependence of the cyclic voltammograms for both reticulated and book-mould electrode structures was recorded in the potential range of −1.5 and −0.5 V (Figure 3(a) and (b)). For both electrodes the anodic–cathodic peak separation increased with scan rate (e.g., from 0.3 V at 50 mV s^{-1} to 0.59 V at 250 mV s^{-1} for the reticulated electrode). Furthermore, the anodic–cathodic peak current ratio was greater than unity. It can be concluded therefore, that the Pb/$PbSO_4$ system exhibits a quasi-reversible behaviour.

The peak potential of the second anodic peak on the reticulated electrode, associated with the PbO sublayer formation, shifted also to more positive values with increasing scan rate (peak a_2 Figure 3(a)).

The dependence of the anodic peak current density $i_{p,a1}$, on the square root of scan rate $v^{1/2}$, reveals interesting differences between the reticulated and conventional grid (Figure 3(a) and (b), insets). A change in slope for $i_{p,a1}$ against $v^{1/2}$ is expected for Pb in H_2SO_4 [19]. In the case of the book-mould electrode, $i_{p,a1}$ became virtually independent of $v^{1/2}$ for scan rates greater than 100 mV s^{-1} (Figure 3(b), inset), whilst for the reticulated electrode there was only a slight decrease in slope (Figure 3(a), inset). The abrupt change of the slope in the case of the conventional grid could be due to the blocked diffusion of SO_4^{2-} through the fast growing and compact sulfate layer [19]. Based on Figure 3(a) and (b), it appears that the sulfate film generated on the reticulated structure is more permeable to both SO_4^{2-} ions and smaller ions such as OH^- and H_3O^+. However, more investigations are needed to verify the latter hypothesis.

3.3. *Cyclic voltammograms representative for the positive battery electrode*

The main electrode reaction at the positive electrode involves the PbO_2/$PbSO_4$ couple (Equation 4). Moreover, the main electrode reaction is accompanied by a

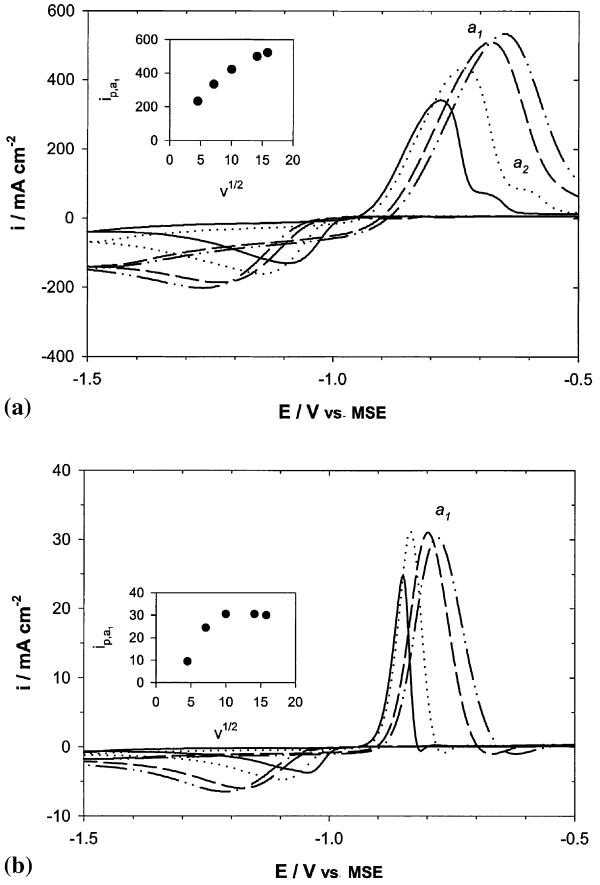

Fig. 3. Influence of scan rate on the cyclic voltammogram representative for the negative battery electrode. Current collector: (a) reticulated and (b) book-mould. $T = 295$ K. Scan rate: (—) 50, (· · · ·) 100, (— —) 200 and (— ··) 250 mV s^{-1}.

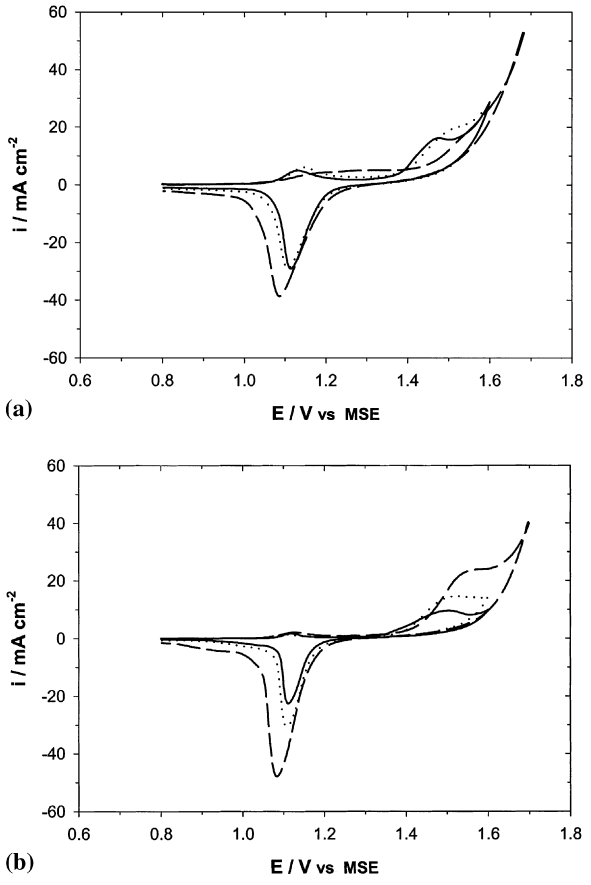

Fig. 4. Influence of scan rate on the cyclic voltammogram representative for the positive battery electrode. Current collector: (a) reticulated and (b) book-mould. $T = 295$ K. Scan rate: (—) 3, (· · · ·) 5 and (— —) 10 mV s^{-1}.

number of secondary reactions related to grid corrosion, oxidation of alloying elements and O_2 evolution (Equation 5) during later stages of charge and overcharge:

$$PbO_2 + 3\,H^+ + HSO_4^- + 2\,e^- \rightleftharpoons PbSO_4 + 2\,H_2O \quad (4)$$

$$2\,H_2O \rightarrow O_2 + 4\,H^+ + 4\,e^- \quad (5)$$

To gain insights into the behavior of the positive battery electrode, cyclic voltammetry experiments were performed on the corrosion layer generated on both reticulated and book-mould grids. The current collector structures were subjected to constant potential electrolysis at +1.15 V vs MSE for three days in H_2SO_4 (rel. density 1.28), afterwards the cyclic voltammograms were recorded (Figure 4(a) and (b)).

On the anodic sweep two peaks were observed for both collectors corresponding to α and β-PbO_2 formation at about 1.1 and 1.5 V, respectively (Figure 4(a) and (b)). The anodic peak current density for α-PbO_2 generation was higher for the reticulated structure; for example, 5 mA cm^{-2} (Figure 4(a)) against 1.8 mA cm^{-2} (grid, Figure 4(b)) at 3 mV s^{-1} scan rate. This suggests that the α-PbO_2 content of the corrosion layer is higher in the case of reticulated collector compared to the conventional grid employed in the present work. The α (orthorombic) crystal modification of PbO_2 is characterized by better electronic conductivity [20], larger crystallite size and smaller surface area [5].

The second anodic peak characteristic for the oxidation of $PbSO_4$ to β-PbO_2, occurred at potentials in the range 1.47 – 1.55 V on the reticulated electrode (Figure 4(a)) and 1.50 – 1.57 V for the conventional grid structure (Figure 4(b)). At 3 and 5 mV s^{-1} scan rate the corresponding peak current density was only slightly higher for the reticulated electrode, while at 10 mV s^{-1} the β-PbO_2 formation and O_2 evolution waves virtually overlapped (Figure 4(a)).

On the cathodic scan both electrodes showed one peak corresponding to PbO_2 reduction to $PbSO_4$, at potentials between 1.11 and 1.08 V for scan rates between 3 and 10 mV s^{-1}.

3.4. *Comparative charge–discharge experiments and figures of merit for the positive active material*

Single cell flooded lead–acid batteries were assembled and formed using either reticulated or book-mould current collectors (Section 2). The charging protocol was

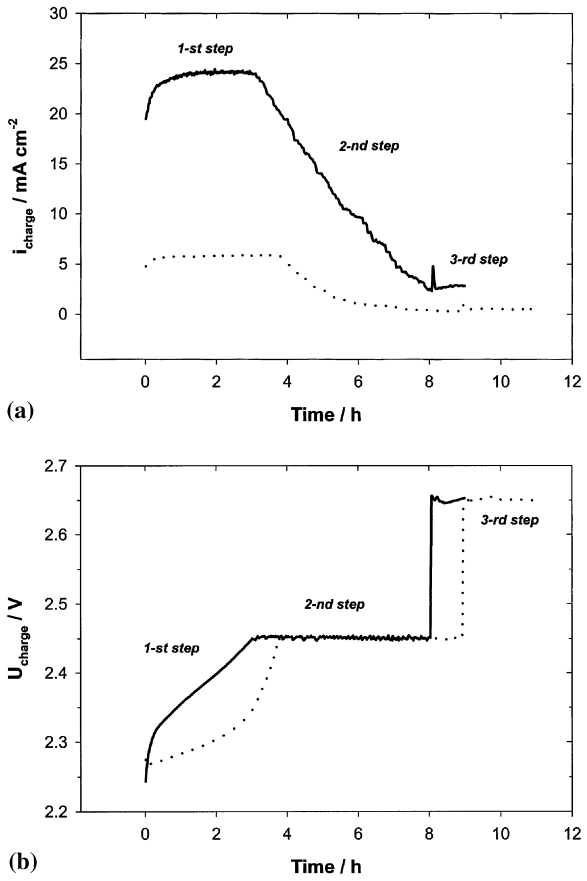

Fig. 5. Comparative charging profiles for the 2 V reticulated and book-mould grid batteries. (a) Superficial charging current density and (b) cell voltage. Key: (—) reticulated; (· · · ·) grid.

composed of three steps: (i) constant current charge at (0.90–0.95) × I_5 with cut-off voltage of 2.45 V; (ii) float charge at 2.45 V until the charging current dropped to 0.1 × I_5; and (iii) equalization charge at 2.65 V for 1 h. The typical charging profiles for the two battery types are presented in Figure 5.

Figure 5(a) shows that over the entire three-step protocol the superficial charging current density was between three to five times higher for the reticulated battery, reaching values as high as 25 mA cm^{-2}. In nine hours, the reticulated battery was recharged by about 120 Ah (kg PAM)$^{-1}$, while the conventional grid battery received only around 90 Ah (kg PAM)$^{-1}$. Thus, the reticulated current collector is better suited for fast charging techniques that require the application of current densities over 20 mA cm^{-2}.

Following charging, the batteries were discharged at the rates and superficial current densities given in Table 2. Figure 6 shows the actual capacities on positive active mass basis for the two battery systems under investigation. At the 5 h rate, the capacity of the positive active mass for the reticulated battery was 115 Ah (kg PAM)$^{-1}$ (Figure 6), corresponding to an electrochemical utilization efficiency of about 51%. Under similar conditions, the capacity of the book-mould grid battery was only 87 Ah (kg PAM)$^{-1}$ and the utilization efficiency

Table 2. Employed superficial discharge current densities

Discharge rate /h	Reticulated collector /mA cm^{-2}	Grid collector /mA cm^{-2}
5	25.6	5.7
4	29.6	6.2
3	37.1	7.2

39%, which is typical for lead acid batteries at the 5 h rate [1]. The difference between the two batteries was more pronounced at the 3 h discharge rate, where the capacity of the positive active mass for the reticulated battery was about 53% higher (i.e., 101 Ah (kg PAM)$^{-1}$ as opposed to 66 Ah (kg PAM)$^{-1}$) for the conventional grid (Figure 6). Correspondingly, the electrochemical utilization efficiency was 45% and 29.5%, respectively.

Typical discharge voltage profiles for the two batteries at the 5 h rate are shown by Figure 7. At the beginning of discharge for both cases a 'voltage-dip' of about 10 to 20 mV was observed, indicative of the $PbSO_4$ crystallization overpotential of fully charged cells [17]. Due to the more than four times lower discharge current density coupled with lower ohmic resistance for a book-mould

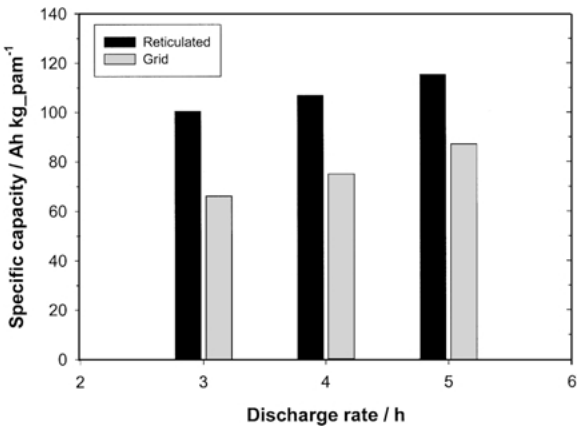

Fig. 6. Specific capacity based on positive active mass.

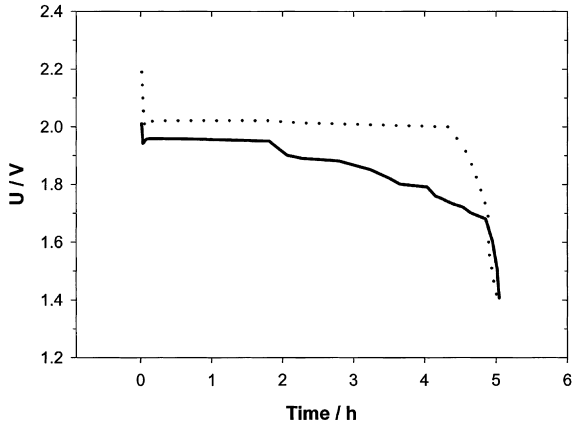

Fig. 7. Voltage profiles during the 5 h discharge rate. Key: (—) reticulated, 25.6 mA cm^{-2}; (· · · ·) grid, 5.7 mA cm^{-2}.

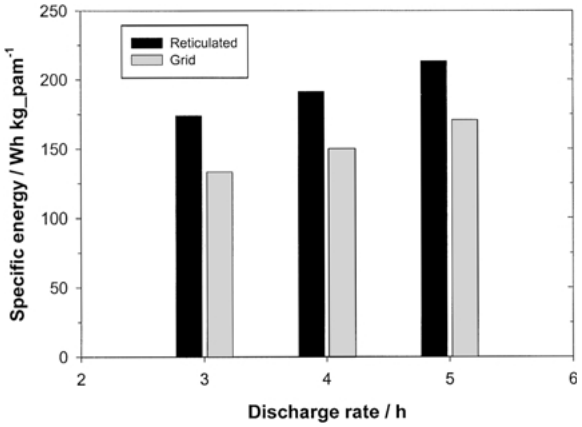

Fig. 8. Specific energy based on positive active mass.

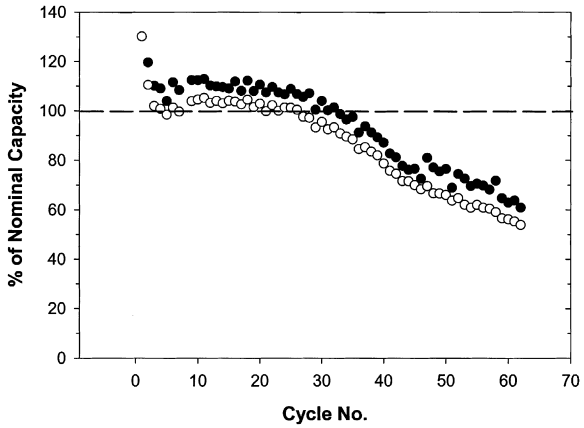

Fig. 9. Cycling of a single-cell reticulated battery with deep discharge. Discharge current density 15.4 mA cm^{-2}, cut-off voltage 1.3 V. Constant voltage charge at 2.4 V for 19 h. Key: (●) charge; (○) discharge.

grid design as opposed to either expanded metal [1] or reticulated structure, the cell voltage of the grid battery was higher and more uniform over the entire 5 h rate. The three-dimensional nature of the reticulated collector (Table 1) coupled with a high discharge current brings about a non-uniform potential distribution in the collector-active material assembly. Further experimental studies coupled with mathematical modeling are required to better understand the current and potential distribution in lead acid batteries with three-dimensional electrodes (i.e., collector-active material system). One of the more practical goals of such an effort would be to determine the 'optimum' thickness or maximum electroactive thickness of the reticulated collectors as a function of important figures of merit such as capacity, specific energy and power.

The specific energies on positive active mass basis are presented in Figure 8. Generally, the reticulated electrodes increased the specific energy by about 30%. For instance, at the 3 h rate the reticulated battery yielded 174 Wh (kg PAM)$^{-1}$, while the specific energy of the book-mould grid battery was 133 Wh (kg PAM)$^{-1}$ (Figure 8). Assuming that a 45% increase in specific energy increases the driving range by 67% [5], extrapolating the data presented in Figure 8, leads to the hypothesis that a battery equipped with reticulated lead current collectors could provide about a 45% longer range.

A preliminary assessment of the deep-cycling performance of the reticulated plates was obtained by subjecting a flooded single-cell battery to successive cycles composed of 19 h constant voltage charge at 2.4 V followed by discharge at 15.4 mA cm^{-2} to a cut-off voltage of 1.3 V. The nominal capacity was calculated at 57% utilization of PAM. This protocol could be relevant for extreme cycling of stand-by batteries.

Figure 9 shows that for thirty cycles the cell was discharged at 100% (or slightly above) of nominal capacity. Between thirty and forty cycles the depth of discharge was above 80% of nominal capacity. With the employed constant voltage charge, the delivered capacity fall below 55% of the nominal capacity after sixty cycles (Figure 9).

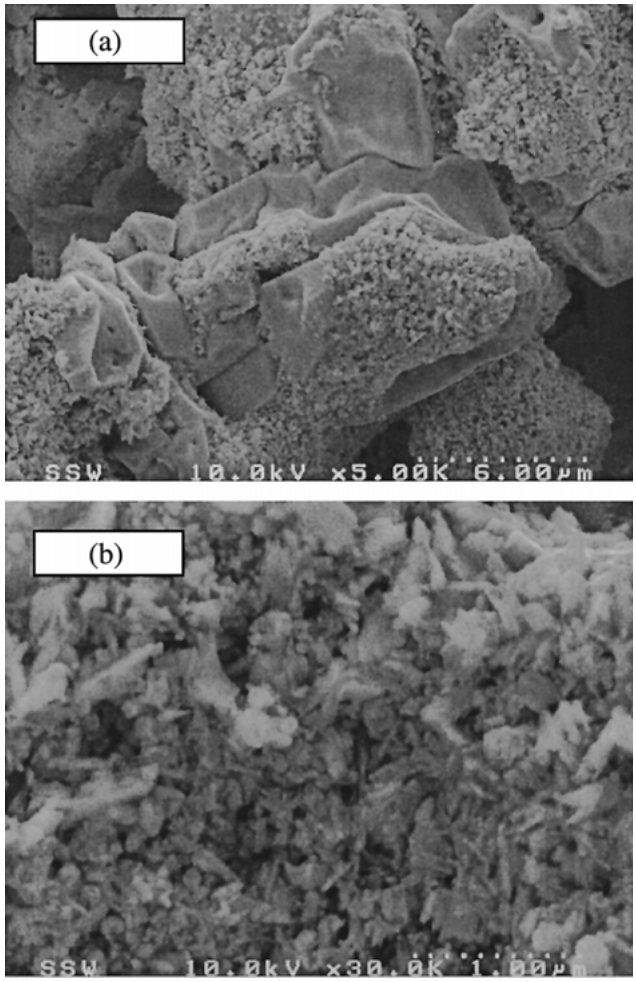

Fig. 10. SEM images of the recharged positive active mass on the book-mould current collector. Resolution: (a) 6 µm, (b) 1 µm; (microstructure of the porous agglomerate).

3.3. *Scanning electron microscopy*

Positive electrodes in recharged state and used for twenty two cycles were subjected to SEM analysis to identify potential differences in the morphology of the

active material induced by the current collector structure. In the case of the book-mould grid, coarse $PbSO_4$ crystals with intergrown, porous PbO_2 agglomerates characterized the appearance of the positive active material structure (Figure 10(a)). On the other hand, the SEM micrograph of the active material on the reticulated electrode (Figure 11(a)) shows significantly more extensive surface coverage by the porous PbO_2 agglomerates with sparsely intercalated, small $PbSO_4$ crystals. The continuous PbO_2 macrostructure on the reticulated substrate allows for a higher utilization efficiency of the active material as compared to a conventional grid.

High resolution SEM images of the porous agglomerate on the reticulated electrode reveal that at a submicrometric level it is composed of both irregular-shaped particles (e.g., plates and grains) of about 0.1–0.2 μm and prismatic, needle-like structures of about 0.3 – 0.5 μm characteristic for α-PbO_2 (Figure 11(b)). Micropores between the crystals are also evident. Similar microstructure was reported for PAM obtained from a $PbO \cdot PbSO_4 + 3PbO \cdot PbSO_4 \cdot H_2O$ paste after extensive cycling [22]. The microstructure of PAM on the book-mould grid (Figure 10(b)), however, appears to be more compact and abundant in structures of plate and grain form (presumably β-PbO_2) as opposed to the network of elongated prismatic crystals observed for the reticulated electrode. It is clear, therefore, that the current collector substrate can have an influence on the active material morphology.

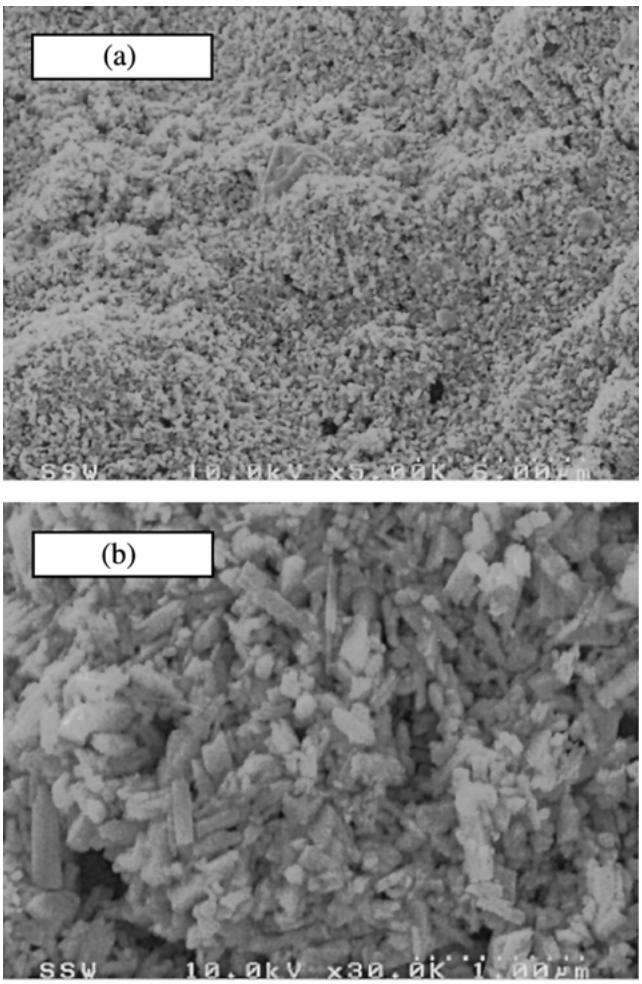

Fig. 11. SEM images of the recharged positive active mass on the reticulated current collector. Resolution: (a) 6 μm, (b) 1 μm; (microstructure of the porous agglomerate).

4. Conclusions

Exploratory studies on the use of high specific surface area reticulated current collectors in lead–acid batteries were performed using cyclic voltammetry, single cell battery testing and scanning electron microscopy. Single cell experiments showed that using three-dimensional reticulated lead collectors increased the electrochemical utilization efficiency of the positive active mass between 30 to 50% during 5 to 3 h discharge rates as compared to conventional book-mould grids. Moreover, the corresponding discharge current densities were as much as five time higher for the reticulated structure (e.g., 37.1 mA cm^{-2} compared to 7.2 mA cm^{-2} (for the grid), at the 3 h rate. Using reticulated current collectors the specific energy per positive active mass improved by about 30% (e.g., at the 3 h rate 174 Wh (kg PAM)$^{-1}$ was obtained as opposed to 133 Wh (kg PAM)$^{-1}$ for the book-mould collector). It is proposed that the above improvement is due mainly to the continuous network of porous active material formed on the reticulated collector as revealed by SEM micrographs.

To complement the present studies, a detailed analysis of corrosion and cycle life behaviour of the reticulated current collectors is required. Furthermore, the optimization of the electroactive thickness for the three-dimensional electrode matrix, based on mathematical modelling in conjunction with experimental studies of the potential and current distribution in the collector-active material assembly, would greatly benefit the development of novel, high-specific energy lead–acid batteries.

References

1. D. Berndt, 'Maintenance-Free Batteries' (Research Studies Press, Taunton, England, 1993).
2. K. Bullock, *J. Power Sources* **51** (1994) 1.
3. (a) R.F. Nelson, *J. Power Sources* **91** (2000) 2; (b) D. Pavlov, *Chinese J. Power Sources* **25** (2001) 9 (Part I) and **25** (2001) 107 (Part II).
4. P.T. Moseley, *J. Power Sources* **80** (1999) 1.
5. D.A.J. Rand, R. Woods and R.M. Dell, 'Batteries for Electric Vehicles' (Society of Automotive Engineers, Warrendale, 1998).
6. S. Ch. Kim and W.H. Hong, *J. Power Sources* **89** (2000) 93.
7. A.D. Turner, P.T. Moseley and J.L. Hutchinson, *in* K.R. Bullock and D. Pavlov (Eds), 'Utilization of Active Material in PbO_2 Electrodes', 'Advances in Lead–acid Batteries', Proceedings Volume 84–14, (The Electrochemical Society, NJ, 1984), pp. 267–273.
8. P. Faber, *in* D.H. Collins (Ed), 'Power Sources 4' (Oriel Press, New Castle upon Tyne, 1973), pp. 525–538.

9. W-H. Kao, N.K. Bullock, and R.A. Petersen, *US Patent 5 302 476*, 12 April (1994).
10. D. Pavlov, *J. Power Sources* **53** (1995) 9.
11. A. Czerwinski and M. Zelazowska, *J. Electroanal. Chem.* **410** (1996) 55.
12. A. Czerwinski and M. Zelazowska, *J. Power Sources* **64** (1997) 29.
13. A. Snaper, *US Patent 6 060 198*, 9 May (2000).
14. J.L. Arias, D.W. Boughn, J.J. Rowlette and E.D. Drake, 16th Annual Battery Conference, Long Beach, CA (2001).
15. ERG Inc., 'Reticulated Vitreous Carbon' (brochure) (1997).
16. R.H. Perry, D. Green and J.O. Maloney (Eds), 'Perry's Chemical Engineers Handbook', 6th edn, (McGraw-Hill, New York, 1984).
17. H. Bode, 'Lead–acid Batteries' (J. Wiley & Sons, New York, 1977).
18. S.M. Caulder and A.C. Simon, 'The Aqueous System Pb^{4+}/Pb^{2+}: Morphological Aspects', *in* A.T. Kuhn (Ed.) 'The Electrochemistry of Lead' (Academic Press, London, 1979).
19. M.A. Dasoyan and I.A. Aguf, 'Current Theory of Lead–Acid Batteries' (Technicopy Ltd, Stonehouse, England, 1979), pp. 281–284.
20. N.A. Hampson, 'The Aqueous System Pb^{4+}/Pb^{2+}: Electrochemical Aspects', *in* A.T. Kuhn (Ed.) 'The Electrochemistry of Lead' (Academic Press, London, 1979).
21. H-T. Liu, J. Yang, H-H. Liang, J-H. Zhuang, W-F. Zhou, *J. Power Sources* **93** (2001) 230.
22. D. Pavlov, E. Bashtavelova and V. Iliev, 'Structure of the lead–acid battery active masses', *in* K.R. Bullock and D. Pavlov (Eds), 'Advances in Lead–acid Batteries', Proceedings Volume 84–14, (The Electrochemical Society, NJ, 1984), pp. 16–32.